Proceedings of the 5th International Symposium on Steel Science (ISSS 2017)
Nov. 13-16, 2017, Kyoto, Japan: The Iron and Steel Institute of Japan

# Current developments in quenched and partitioned steels

Emmanuel De Moor[1*], Joonas Kähkönen[1], Preston Wolfram[1], John G. Speer[1]

[1] Advanced Steel Processing and Products Research Center,
Colorado School of Mines
1500 Illinois Street
Golden, CO-80401, USA

**Abstract:** Quenching and partitioning (Q&P) is receiving significant attention from the steel research, producing, and using communities. The present contribution reviews Q&P fundamentals and provides an update on current findings in the authors' laboratory related to physical metallurgical investigations related to carbon partitioning, with particular emphasis on mechanisms competing with carbon partitioning from martensite into austenite such as transition carbide precipitation. A discussion of alloying effects associated with elevated manganese and carbon levels is also included. In addition, although the bulk of the Q&P work has been focused towards automotive applications, perspectives are given on other potential applications such as abrasion resistant grades. In this context, dry sand rubber wheel testing results of Q&P processed steels with varying retained austenite levels and fixed hardness levels are discussed.

## 1. INTRODUCTION

Quenching and partitioning (Q&P) consists of a rapid quench from the annealing temperature, which can be in the intercritical or austenitic region, to a so-called quenching temperature (QT), intermediate to the martensite start ($M_s$) and finish ($M_f$) temperatures followed by isothermal holding at the quench temperature or at an elevated temperature, the partitioning temperature (PT), and quenching to room temperature [1,2]. The former approach is referred to as one-step Q&P while the latter two-step Q&P. The intent of the partitioning step is to carbon-enrich the austenite to stabilize it to room temperature. A microstructure consisting of a martensitic matrix and retained austenite is therefore obtained. The quenching temperature is an important parameter for Q&P processing as it governs the amount of martensite and austenite present in the microstructure before the partitioning treatment starts. Note that this temperature also governs the potential level of carbon enrichment of the austenite since the amount of carbon available for enrichment is proportional to the amount of martensite present at that temperature. A methodology has been developed to calculate the austenite fractions that can be stabilized assuming full carbon partitioning from martensite into austenite and to determine the "optimum" quenching temperature which corresponds to the greatest austenite fraction [2]. The present contribution will review some of the work performed recently pertaining to microstructural aspects of Q&P steels, effects of carbon and manganese on tensile properties, and abrasion wear performance.

## 2. MICROSTRUCTURAL EVOLUTION

Results of the aforementioned calculation are shown in Fig. 1 for a 0.28C-1.48Mn-1.48Si steel as the solid line [3]. Full austenitization was assumed and an optimum QT of 240 °C was predicted. In addition, experimental data are shown, obtained by X-ray diffraction, of the retained austenite fractions in samples Q&P processed following reheating at 860 ºC for 120 s and two-step Q&P using a partitioning temperature of 400 ºC and holding (partitioning) times (Pt) of 10, 30, 60 and 300 s. A discrepancy between the calculated and experimentally measured fractions exists where significantly lower fractions are observed for certain quenching temperatures which may relate to the assumptions embedded in the model calculations and mechanisms actively competing for the available carbon.

Example evolution of retained austenite fractions with partitioning time is shown in Fig. 1b for 0.24C-1.61Mn-1.45Si and 0.25C-1.70Mn-0.55Si-0.69Al samples [4]. Silicon and aluminium are added to suppress cementite as its formation is not desired given the associated carbon consumption which reduces its availability for enrichment in austenite. The fractions were measured using magnetic

* Corresponding author. E-mail: edemoor@mines.edu, telephone: +1 303 273 3624.

saturation in the Figure 1b and varying partitioning temperatures of 350, 400, and 450 ºC were employed. Decreasing trends with increasing partitioning time are observed for both alloys. In general, the austenite fractions are lower in the aluminum containing alloy and the fractions decrease more gradually in the CMnSi alloy with partitioning time. A review of effects on Q&P response of other alloying additions can be found in [5].

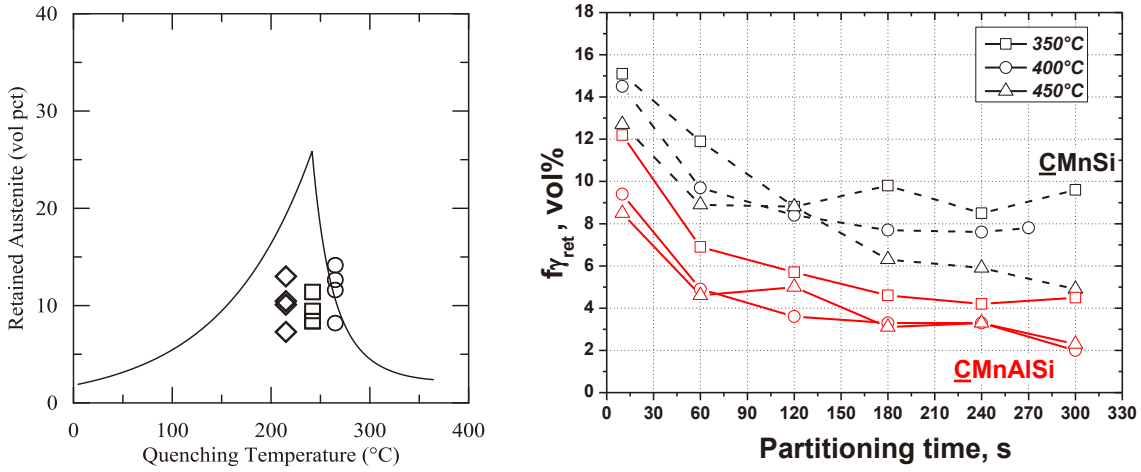


a) b)

Fig. 1. Retained austenite fractions a) calculated assuming full carbon depletion of the martensite (solid line) and measured by X-ray diffraction (discrete data points) in 0.28C-1.48Mn-1.48Si Q&P samples as a function quenching temperature with partitioning performed at 400 ºC for times ranging from 10 to 300 s and b) obtained by magnetic saturation measurements as a function of partitioning time in 0.24C-1.61Mn-1.45Si and 0.25C-1.70Mn-0.55Si-0.69Al samples processed by Q&P with partitioning at the indicated temperatures. Full austenitization preceded quenching in both studies. Figures reproduced from [11] and [4].

Fig. 2 shows combined electron backscatter diffraction (EBSD) phase and image quality maps of a one-step 0.25C-2Mn-1.5Si Q&P sample held at a QT of 300 ºC for 300 s in addition to a sample isothermally held in the vicinity of the $M_s$ temperature at 450 ºC for 120 s [6]. The latter heat treatment reflects a TRIP bainitic ferrite type approach. The morphologies of the retained austenite are clearly different with the Q&P sample being thin film-like (and largely unresolved) whereas the austenite shown in Fig. 2b is more blocky. More austenite is retained following holding at 450 ºC and an overall coarser microstructure has developed.

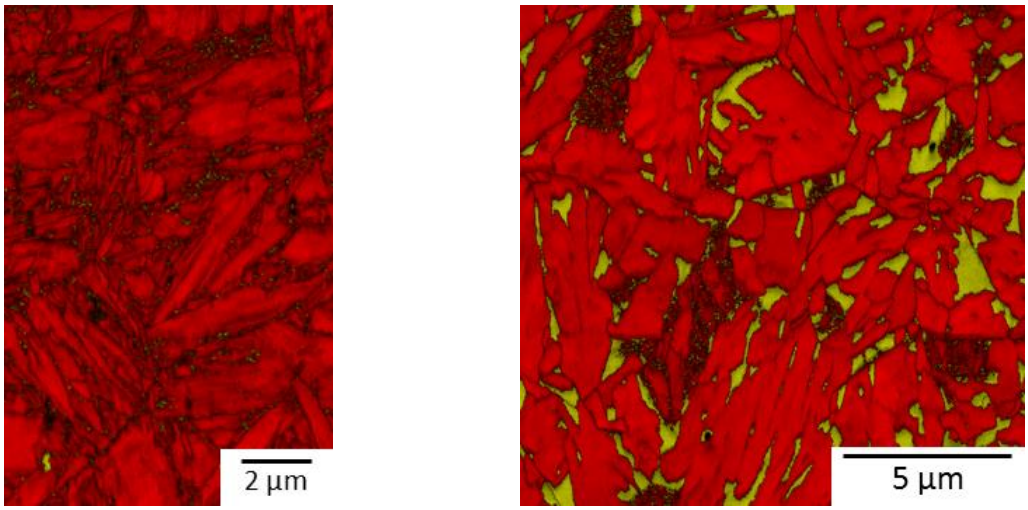


a) b)

Fig. 2 Combined phase and image quality maps for 0.25C-2Mn-1.5Si samples heat treated by a) one-step Q&P using a QT of 300 ºC and a 300 s hold and b) isothermal holding slightly below the $M_s$ temperature at 450 ºC for 120 s following full austenitization at 900 ºC for 150 s. Figures reproduced from [6].

A montage of bright field transmission electron micrographs from a 0.20C-1.63Mn-1.63Si Q&P sample partitioned at 300°C for 120s is given in Fig. 3. Lath martensite with a high dislocation density is apparent and transition carbides are clearly observed in one of the martensite laths. Although these carbides do not have a detrimental effect on mechanical properties, their presence is not necessarily desired since they act as carbon "sinks" and therefore reduce the capacity for partitioning of carbon into austenite and austenite stabilization. In order to further understand this competition, quantitative analysis of transition carbides in Q&P samples was recently performed by Mössbauer spectroscopy [7,8,9,10].

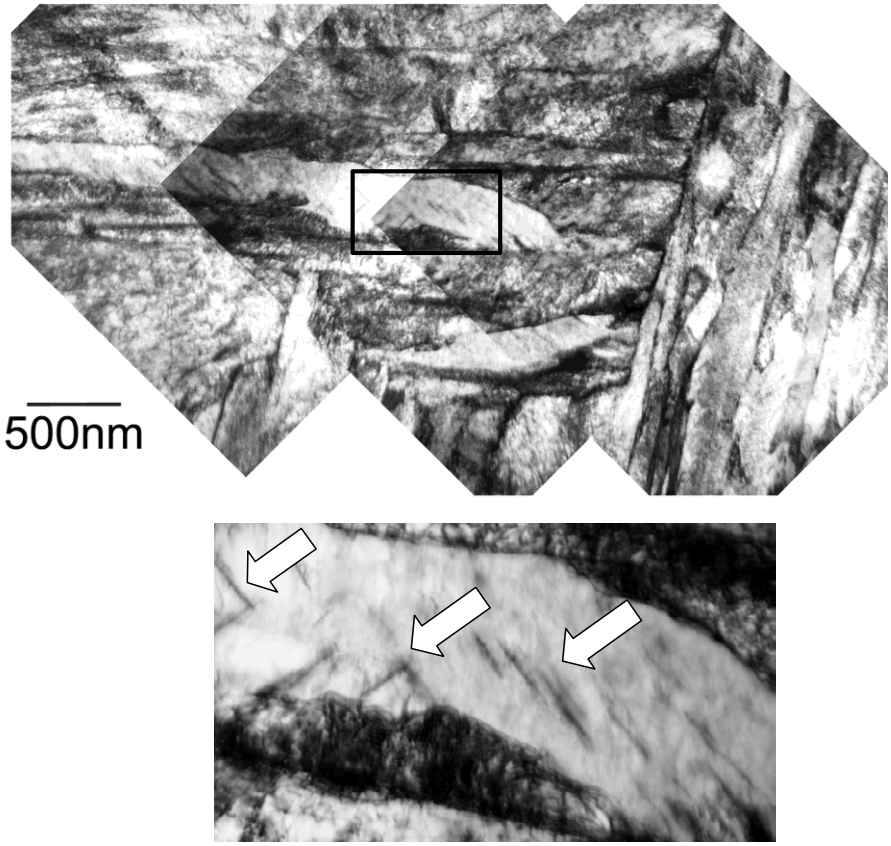


Fig. 3. Bright field transmission electron micrograph of a 0.20C-1.63Mn-1.63Si Q&P microstructure (QT: 240°C, PT: 300°C, Pt:120s) showing the presence of transition carbides.

Fig. 4 shows results of Mössbauer analysis for 0.38C-1.54Mn-1.48Si samples partitioned at two temperatures, 400 and 450 ºC, as a function of partitioning time and hold (reflecting the time at the QT) time [8]. The amounts of austenite, η transition carbides, and cementite were determined by the Mössbauer analysis methodology detailed in [7,8]. The left hand side figures show the results for partitioning at 400 ºC whereas the right hand side figures show the data obtained following partitioning at 450 ºC. η transition carbides were detected by Mössbauer spectroscopy for both partitioning treatments and a modest increase with partitioning time is apparent as shown in Fig. 4a and d. The presence of η carbides was also confirmed by TEM [7,8]. Additionally, cementite was observed when partitioning at 450 ºC for times of 60 s and longer. Fig. 4b and e show the evolution of the austenite amount and its carbon content with partitioning time. For both partitioning temperatures a maximum is observed. It is interesting to note that the decrease in austenite fractions for the 450 ºC partitioning conditions occurs simultaneously with the appearance of cementite. It is unclear, however, whether this cementite is associated directly with austenite decomposition or with formation in the martensitic laths. No direct microscopic evidence was found for cementite as an austenite decomposition product although austenite decomposition into ferrite/cementite would certainly contribute to increased cementite fractions. As the Mössbauer results quantify transition carbides, cementite and austenite amounts and their respective carbon contents, the carbon content remaining in the martensite can be estimated by a mass balance calculation. The results of this approach are shown in Fig. 4c and f where the carbon in

the various phases is reported as a fraction of the total (bulk) carbon content. Approximately 0.20 of the total bulk carbon is present in transition carbides after partitioning for 10 s at 400 ºC and the fraction increases with partitioning time. Partitioning at 450 ºC initially results in lower carbon fractions in the transition carbides as compared to the lower partitioning temperature, followed by substantial increases up to 0.7 as cementite formation occurs. Up to approximately half of the bulk carbon is present in the austenite for both partitioning temperatures. Continuously decreasing carbon levels are observed in the martensite with partitioning time and a more pronounced decrease is initially observed for the 450 ºC partitioned samples.

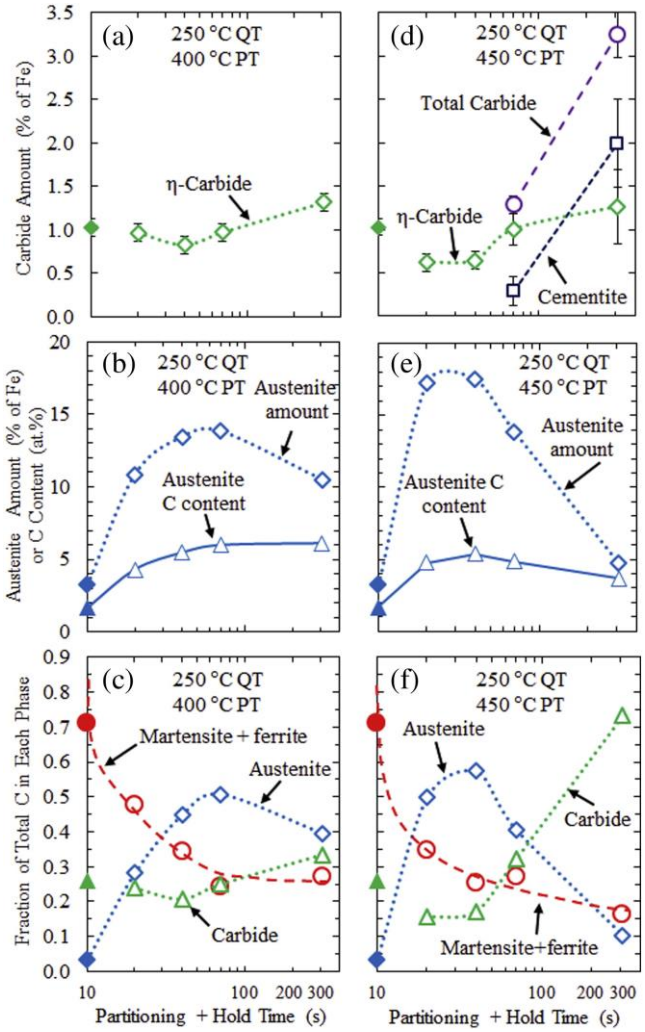


Fig. 4. Mössbauer results for 0.38C-1.54Mn-1.48Si samples fully austenitized at 820 ºC for 120 s, quenched to 250 ºC and held for 10 s, and partitioned at 400 ºC (a, b, c) or 450 ºC (d, e, f). a) and d) amount of carbides, b) and e) amount of austenite and austenite carbon content, and c) and f) fraction of total carbon in austenite, carbides, and martensite/ferrite as a function of partitioning and hold time. Open symbols are two-step Q&P and filled symbols are one-step Q&P processed samples. Figure reproduced from [8].

## 3. TENSILE PROPERTIES

It is interesting to note and confirm that strength levels of Q&P steels depend on the carbon content in the martensite as suggested by consideration and comparison of Fig.4f and Fig. 5a. The latter figure shows ultimate tensile strengths plotted as a function of partitioning time. The carbon content in martensite shown in Fig.4f obtained by the mass balance calculation discussed earlier shows an overall similar trend with partitioning time as the ultimate tensile strength presented in Fig. 5a.

Fig. 5b shows tensile properties of CMnSi Q&P samples (PT: 400 ºC and Pt: 10, 300 s) with varying bulk carbon contents ranging from 0.2 to 0.4 wt pct while manganese and carbon levels were fixed at approximately 1.5 wt pct [3,11,12]. Increasing carbon levels clearly increase strength whereas tensile ductility appears less affected. This is in contrast to the effect of manganese alloying reflected in Fig.

6a, which shows increased strength and tensile elongation with increased bulk manganese content over the range from 1.5 to 5 wt pct for 30 s partitioning at 400 ºC and a fixed carbon content of approximately 0.3 wt pct [11]. Substantial tensile elongation develops when the manganese level is increased from 1.5 to 3 wt pct whereas similar tensile ductility is obtained, albeit at higher ultimate tensile strength, at a manganese level of 5 compared to 3 wt pct. Further work remains to help understand the role of manganese affecting tensile properties and austenite retention including the martensite/austenite interface migration. A summary of the results of an expanded study for these alloys is shown in Fig. 6b where the effect of an increase in manganese content from 1.5 to 3 wt pct is again observed whereas a further increase to 5 wt pct provides a less pronounced improvement of tensile property combinations. It is noteworthy that ultimate tensile strengths ranging from 1500 to 1600 MPa with total elongations of 20 pct were obtained.

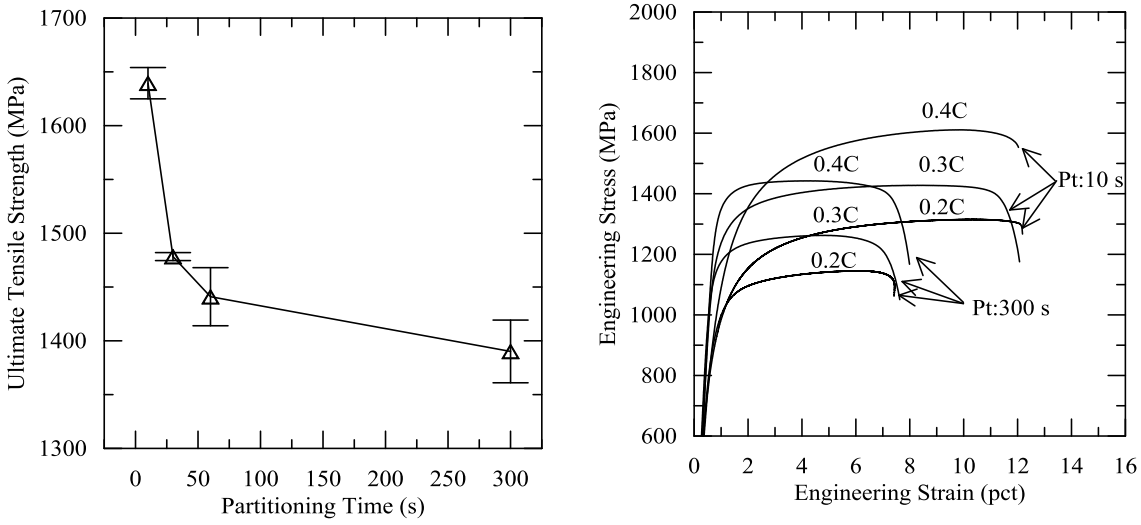


Fig. 5. a) Ultimate tensile strength as a function of partitioning time for 0.38C-1.54Mn-1.48Si samples fully austenitized at 850 ºC for 120 s quenched to 250 ºC and partitioned at 400 ºC. b) Engineering stress-strain curves for 0.20C-1.63Mn-1.63Si (0.2C, QT: 240 ºC), 0.29C-2.95Mn-1.59Si (0.3C, QT: 240 ºC), and 0.38C-1.54Mn-1.48Si (0.4C, QT: 225 ºC) samples partitioned at 400 ºC for 10 or 300 s. Figures reproduced from [3,11].

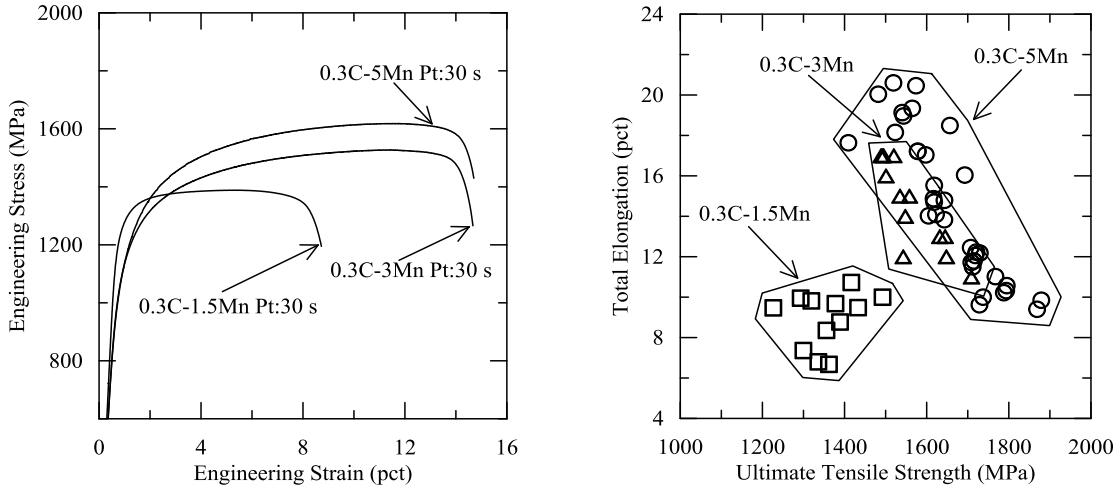


Fig. 6. a) Engineering stress versus strain curves for 0.28C-1.48Mn-1.48Si (0.3C-1.5Mn), 0.29C-2.95Mn-1.59Si (0.3C-3Mn), 0.29C-4.96Mn-1.64Si (0.3C-5Mn) Q&P samples partitioned at 400 ºC for 30 s. b) Total elongation versus ultimate tensile strength combinations generated in the same alloys. Figures reproduced from [11].

## 4. WEAR BEHAVIOR

The better combinations of properties shown in Fig. 6b are of substantial interest to the automotive industry as material alternatives enabling room temperature forming operations at strength levels currently obtained by hot stamping may be viable. Opportunities may exist, however, beyond automotive applications. As an example, Fig. 7 shows the wear performance of alloy 9260 (with composition 0.60C-0.95Mn-1.96Si (wt pct)) heat treated samples as measured by the weight and associated volume loss during dry sand rubber wheel (DSRW) wear testing according to ASTM G 65 Procedure B [13]. Heat treating details of the various samples are provided elsewhere [14] and the results were compared and normalized with respect to the performance of an AR400F (abrasion resistant) grade with composition 0.14C-1.37Mn-0.12Si-0.14Ni-0.15Cr-0.15Mo-0.03Ti-0.03Al-0.002B (wt pct). Fig. 7a plots the normalized volume loss as a function of hardness and a continuously decreasing trend of improved wear performance with increasing hardness is noted, as commonly reported. Fig. 7b shows the wear performance as a function of retained austenite content for a fixed hardness level of 60 ± 1 HRC indicating a beneficial effect of the presence of austenite. The sample without retained austenite was quenched and tempered to the hardness level.

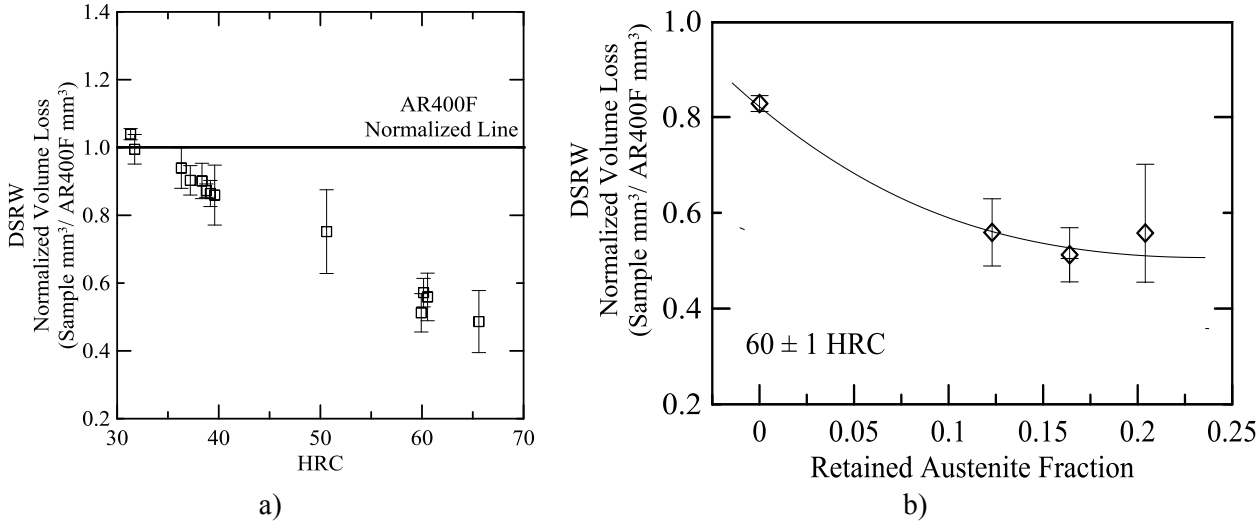


Fig. 7. Volume loss of 9260 Q&P samples normalized with respect to the performance of AR400F samples during dry sand rubber wheel wear testing (DSRW) plotted a) as a function of Rockwell hardness on the C scale (HRC) and b) as a function of retained austenite fraction at a fixed hardness level of 60 ± 1 HRC. Figures reproduced from [14].

While automotive steels have received the most attention in the Q&P steel development community, heavier gauge products may be of interest in future development and applications [15]. Q&P fundamental work remains to apply carbon partitioning strategies in environments which are constrained by product thickness or geometry in different product forms which do not allow fast, uniform cooling and/or isothermal partitioning. Thomas [16] has developed the concept of non-isothermal partitioning during coil cooling of a hot rolled product and Stewart is applying Q&P concepts to processing of plate steels [17].

## 4. CONCLUSIONS

A brief overview of current activities pertaining to quenching and partitioning steels was presented, in particular related to microstructural evolution during Q&P processing, tensile properties and wear performance. A study using Mössbauer spectroscopy of the phase fractions and their carbon contents was reviewed. Increased carbon alloying results in strength increases without affecting tensile elongation, whereas manganese alloying increases both ultimate tensile strength and tensile elongation in particular when manganese levels are increased from 1.5 to 3 wt pct. Attractive properties with tensile strength levels in excess of 1500 MPa and total elongations of 20 pct were obtained. In addition to tensile properties, wear performance was considered, and a beneficial effect of retained austenite seems apparent.

**Acknowledgements:** The support of the sponsors of the Advanced Steel Processing and Products Research Center is gratefully acknowledged. This material is partially based upon work supported by the Department of Energy Advanced Manufacturing Office under Award Number DE-EE0005765.



## REFERENCES

[1] J.G. Speer, D.K. Matlock, B.C. De Cooman, and J.G. Schroth: Acta Mater., 51 (2003) 2611-2622.
[2] J.G. Speer, A.M. Streicher, D.K. Matlock, F. Rizzo, and G. Krauss: Austenite Formation and Decomposition (ed. by E.B. Damm and M.J. Merwin) TMS, Warrendale, PA (2003) 505-522.
[3] J. Kähkönen: MS thesis, Colorado School of Mines, Golden, CO (2016).
[4] E. De Moor, J.G. Speer, D.K. Matlock, C. Föjer and J. Penning: Proc. Materials Science and Technology(MS&T) 2009, The Printing House, Inc., Stoughton, WI (2009) 1554-1563.
[5] E. De Moor and J.G. Speer: "Bainitic and Quenching and Partitioning Steels," Chapter 10 in Automotive Steels, (ed. by R. Rana and S.B. Singh) Woodhead Publishing Series in Metals and Surface Engineering, Woodhead Publishing, an imprint of Elsevier Ltd., (2017) 289-316.
[6] R.J. Johnson, E. De Moor, N. Fonstein, D.N. Hanlon, A. Pichler: Proc. Int. Symp. on New Developments in Advanced High-Strength Sheet Steels (ed. by E. De Moor, H.J. Jun, J.G. Speer, and M. Merwin) AIST, Warrendale, PA, (2013) 71-83.
[7] D.T. Pierce, D.R. Coughlin, D.L. Williamson, K.D. Clarke, A.J. Clarke, J.G. Speer and E. De Moor: Acta Mater., 90 (2015) 417-430.
[8] D.T. Pierce, D.R. Coughlin, D.L. Williamson, J. Kähkönen, A.J. Clarke, K.D. Clarke, J.G. Speer, E. De Moor: Scripta Mater., 121 (2016) 5-9.
[9] D. T. Pierce, D. R. Coughlin, D. L. Williamson, K. D. Clarke, A. J. Clarke, J. G. Speer, D. K. Matlock, E. De Moor: Micro. and Microanal. (2015) 2271-2272.
[10] D.T. Pierce, D.R. Coughlin, D.L. Williamson, K.D. Clarke, A.J. Clarke, J.G. Speer, D.K. Matlock and E. De Moor: Proc. of the Intl. Conf. on Solid-Solid Phase Transformations in Inorganic Materials, (ed. by M. Militzer, G. Botton, L.-Q. Chen, J. Howe, C. Sinclair, and H. Zurob) (2015) 91-98.
[11] M.J. Kähkönen, E. De Moor, J. Speer and G. Thomas: SAE J. Mater. Manuf., 8(2), (2015) 419-424.
[12] E. De Moor, J. Kähkönen, J.G. Speer and D.K. Matlock: Proc. of the 9th Intl. Conf. on Advanced Materials and Processing (PRICM9), (ed. by T. Furuhara, M. Nishida and S. Miura) The Japan Institute of Metals and Materials (2016) 167-170.
[13] Standard Test Method for Measuring Abrasion using the Dry Sand/rubber Wheel Apparatus, ASTM standards: G 65-94.
[14] P. Wolfram, MS Thesis, Colorado School of Mines, Golden, CO (2013).
[15] W. Wang, H.-R. Wang, S. Liu and A. Yang, : Proc. of the 9th Intl. Conf. on Advanced Materials and Processing (PRICM9), (ed. by T. Furuhara, M. Nishida and S. Miura) The Japan Institute of Metals and Materials (2016) 108-113.
[16] G. A. Thomas, J. G. Speer, and D. K. Matlock: Metall. and Mater. Trans. A, 42(12), (2011) 3652-3659.
[17] R.A. Stewart, J.G. Speer, B.G. Thomas, A.J. Clarke, E. De Moor: Proc. AISTech 2017, AIST, Warrendale, PA (2017) 2881-2892.